A. Colagrossi, J. Prinetto, S. Silvestrini, M. Lavagna
Sky Visibility Analysis for Astrophysical Data Return Maximization in HERMES Constellation
Journal of Astronomical Telescopes, Instruments, and Systems, Vol. 6, N. 4, 2020, 048001 (25 pages)
doi:10.1117/1.JATIS.6.4.048001

Sky visibility analysis for astrophysical data return maximization in HERMES constellation

Andrea Colagrossi,* Jacopo Prinetto, Stefano Silvestrini, and Michèle Lavagna
Politecnico di Milano, Milano, Italy

Abstract. HERMES is a scientific mission composed of 3U nanosatellites dedicated to the detection and localization of high-energy astrophysical transients, with a distributed space architecture to form a constellation in Earth orbits. The space segment hosts novel miniaturized detectors to probe the x-ray temporal emission of bright events, such as gamma-ray bursts, and the electromagnetic counterparts of gravitational wave events, playing a crucial role in future multimessenger astrophysics. During operations, at least three instruments separated by a minimum distance shall observe a common area of the sky to perform a triangulation of the observed event. An effective detection by the nanosatellite payload is achieved by guaranteeing a beneficial orbital and pointing configuration of the constellation. The design has to cope with the limitations imposed by small space systems, such as the lack of on-board propulsion and the reduced systems budgets. We describe the methodologies and the proposed strategies to overcome the mission limitations, while achieving a satisfactory constellation visibility of the sky throughout the mission duration. The mission design makes use of a high-fidelity orbit propagator, combined with an innovative mission analysis tool that estimates the scientific performances of the constellation. The influence of the natural relative motion, which is crucial to achieve an effective constellation configuration without on-board orbit control, is assessed. The presented methodology can be easily extended to any kind of distributed scientific space applications, as well as to constellations dedicated to Earth and planetary observation. In addition, the visibility tool is applicable in the context of the constellation flight dynamics operations, yielding optimized results and pointing plans based on actual satellite orbital positions. [DOI: 10.1117/1.JATIS.6.4.048001]

Keywords: astrophysical transients localization; nanosatellite constellation; scientific performances optimization; natural relative dynamics; distributed space system.

Paper 20035 received Apr. 10, 2020; accepted for publication Sep. 22, 2020; published online Oct. 9, 2020.

1 Introduction

HERMES is a scientific space mission dedicated to the detection and localization of high-energy astrophysical transients, such as gamma-ray bursts (GRBs), and of the electromagnetic counterparts of gravitational wave events (GWEs), whose detection probability is increased by distributing numerous sensors on Earth-bounded orbits. Therefore, a constellation of 3U nanosatellites is implemented to guarantee the distributed satellites architecture. During operations, at least three spacecraft, in the required configuration, shall observe GRBs events to perform triangulation and get a significant scientific content from the differential measurements.[1]

HERMES space segment is composed of a distributed architecture of 3U spacecraft to fly on low Earth orbit. The science operations scenario is identified by means of analyses concerning the visibility of the sky and, thus the expected number of GRBs in view of HERMES constellation. The operational orbit and the injection strategy of the elements of the constellation determine the dynamics and the evolution of the relative orbits of the spacecraft. In addition, the pointing strategy is crucial to perform the alignment of the scientific instruments field of view (FOV). The FOV alignment, together with the mutual distances between the spacecraft

*Address all correspondence to Andrea Colagrossi, E-mail: andrea.colagrossi@polimi.it

2329-4124/2020/$28.00 © 2020 SPIE

(i.e., physical baseline), yields to the distance projected along the pointing direction of the scientific instruments (i.e., projected baseline). Furthermore, the effective GRBs detection by the nanosatellite payload is achieved by respecting numerous feasibility constraints on the orbital and pointing configuration of the spacecraft. The feasible projected baseline is evaluated to assess the fulfillment of the scientific objective, allowing to determine the region of the sky that can be triangulated and, hence, the expected number of triangulated GRBs.

The current phase of the mission development is focused on the implementation of a technological pathfinder (TP) and a scientific pathfinder (SP) using a reduced constellation of $3 + 3$ nanosatellites to be launched in 2021. HERMES-TP was selected by the Italian Ministry of University and Research supported by the Italian Space Agency, to design, integrate, and test the first three nanosatellites. HERMES-SP, funded by the EC-H2020, extended the constellation with an SP of additional three space elements. The options to launch the six satellites with a single launch or with two separate launches are still open, and the mission design had to cope with this variability.

This paper describes the methodologies and the proposed strategies to cope with HERMES constellation, in the complete six spacecraft configuration. The limitations imposed by the small space system, such as the lack of on-board propulsion and the reduced systems budgets, shall be overcome, while achieving a satisfactory constellation visibility of the sky throughout the mission duration. The proposed methodology combines a high-fidelity orbit propagator, including all the major environmental perturbations, with a sky visibility tool that analyzes the scientific constraints based on relative positions and pointing directions. The tool allows to perform the analysis of the preliminary constellation in any orbital scenario. Moreover, the investigation entails the possibility to compare different pointing strategies for the spacecraft, in order to select the nominal attitude motion that maximizes the visibility time. The presented tool is useful for flight dynamics operations planning, being flexible enough to be able to utilize in-flight data to generate optimal pointing schedules. The influence of the orbital injection of the nanosatellites, both for a single and separate launch, is assessed in terms of the evolution of relative motion and achievable observation time. A propulsion system is not available; hence, it is critical to leverage natural motion and differential perturbations to achieve the desired configuration. The available results and the presented mission design work serve as a basis to implement an extended full constellation (FC) of N satellites that will compose HERMES-FC.

This research represents the basis for the design of satellite constellations dedicated to the observation of the sky, maximizing the coverage with numerous scientific detectors available. This is becoming particularly relevant for small satellites mission, whose advantage is based on the possibility to exploit a distributed system composed of many simple elements, rather than a unique scientific detector with advanced system capabilities. For this reason, the mission analysis shall exploit innovative techniques and tools capable to boost the constellation performances, while respecting the typical scientific requirements and the small system limitations.

The methods proposed in this paper are suitable for nanosatellites distributed scientific applications, easily configurable to include any kind of scientific requirement that can be formulated as a mathematical relation. Moreover, the possibility to investigate the available scientific performances considering the natural relative dynamics is crucial for small-space platforms without on-board propulsion.

The developed tools can be further generalized to distributed missions dedicated to Earth and planetary remote sensing observation, being pointing direction and FOV of the scientific instruments completely configurable as per system and mission requirements. The proposed analytical optimization technique can easily include ground related scientific merit parameters, as long as they can be defined with mathematical sets and formulas, as will be described for the proposed HERMES applicative case in Sec. 3.

In summary, the intended scientific contribution of the paper can be summarized as follows.

- To present the mission design for the HERMES constellation. In particular, being a nanosatellite mission, smart solutions are required to solve the shortcomings arising from limited mission resources (e.g., no orbital control and limited launch budgets).
- To describe the development of a sky visibility tool to assess scientific mission yield. The tool can be utilized by both constellation designer and operators to predict mission outcome or generate optimal pointing plans with respect to sky visibility performances.

- To analyze different optimal pointing philosophies in terms of number of detected GRBs, sky regions coverage, and triangulation accuracy.
- To investigate the effect of number and frequency of spacecraft maneuvers required to change the payload pointing directions.
- To investigate the robustness of the mission architecture against expected uncertainties and the possible extension of the proposed design, providing useful insights for future nanosatellite constellation designer.

The remainder of this paper is structured as follows. Section 2 presents a discussion on orbital injection strategies, analyzing the main gravitational perturbations in low Earth orbit, to highlight the most effective way to achieve the desired intersatellite baseline, within the existing limitations in launch opportunity for small space systems. Section 3 describes the methods and the developed tool to analyze the sky visibility of the constellation, associated with certain instrument pointing directions. Section 4 discusses the effects of the definition and planning of the operational pointing directions on the astrophysical data return. In particular, the differences in GRB triangulation accuracy and in sky coverage are presented, as well as the influence of the pointing variations frequency. This section also presents the pointing directions optimization algorithm, designed to improve the scientific outcomes of the mission. Section 5 presents the proposed HERMES constellation scenario. The robustness of the selected design strategies, with respect to mission uncertainties, is assessed with a statistical analysis. Different pointing strategies are compared to select the one providing the greater scientific results. Moreover, the guidelines to extend the constellation design to a larger FC are discussed.

1.1 *Scientific Requirements*

HERMES payload is a simple but innovative detector[2] to probe the x-ray and gamma-ray emission of bright high-energy transients. It is hosted in a single CubeSat Unit (1U), and the detector assembly is primarily composed of 60 scintillator crystals and 12 silicon drift detectors (SDD) arrays, each with 10 independent cells. Both SDDs and crystals are employed to detect high-energy photons, the former in the x-ray range, the latter in the gamma-ray range. The crystals are optically connected to the SDDs, and each crystal is read out by two SDD cells. The detectors are supported by a dedicated mechanical structure, a payload data handling unit, a power supply unit, and an optical filter, to provide effective filtering of visible and UV-IR emissions. The payload is designed and assembled by the Italian National Institute of Astrophysics (INAF), which is also responsible for the payload operations.

HERMES mission design is strongly characterized by the payload operations as well as the set of mission and scientific requirements. In particular, since a minimum number of GRBs shall be detected simultaneously by at least three space elements, the main scientific requirements affect the baseline between the satellites and the alignment of their FOVs. Formally, the requirements are as follows.

- At least three satellites shall have common FOV, within ± 60 deg to maintain 50% efficiency in the detector field.
- The physical baseline between at least three co-observing satellites shall be >1000 km.
- At least two couples of co-observing satellites shall have the baseline projected along the mean pointing direction of the scientific instruments >1000 km.

These requirements shall be satisfied within the HERMES system possibilities. In fact, HERMES satellites are equipped with complete attitude control subsystem, but no propulsion unit is presented on-board. Therefore, the pointing direction of the payload and the FOV overlap can be controlled, but the physical baseline between the satellites shall be guaranteed by means of natural dynamics only.

Additional scientific requirements led to constraints on the operational orbit of the constellation: detector lifetime is limited by the leakage current, which depends on the radiation environment, which is a function of orbit altitude and inclination. The requirements applied for the orbit design are as follows.

- The mission duration shall be >2 years.
- The altitude of the operational orbit shall be <600 km.
- The inclination of the operational orbit shall be <30 deg or >70 deg.

The first requirement can be translated in a lower bound for the orbit altitude: a HERMES spacecraft, with a mass to area ratio in the order of $\sim 50\ \mathrm{kg/m^2}$, has an orbital lifetime >2 years for an initial orbit altitude >450 km, with average solar activity (i.e., $F10.7 \sim 100$ sfu).[3,4] Hence, the orbit design process is constrained to nearly equatorial orbit or Sun synchronous orbit (SSO) with $450\ \mathrm{km} \leq h \leq 600\ \mathrm{km}$.

1.2 *Orbital Simulator*

The mission design relies on accurate modeling of the satellite orbital motion. In particular, the dynamical model shall be accurate enough to catch the natural relative dynamics between the spacecraft of HERMES constellation. The methods and the analyses presented in this paper are supported by an orbital propagator, developed, and validated by the authors at Politecnico di Milano. The dynamical model takes into account all relevant perturbing forces acting in low Earth orbits, namely as follows.

- *Earth geopotential based on EGM96 model*. The accepted truncation error for the spherical harmonic order at the given altitude is selected according to the intrinsic accuracy of the EGM96 model, as per ECSS guidelines.[5,6]
- *Solar gravitational perturbation*. Sun's position is based on DE431 Ephemeris model.[7]
- *Lunar gravitational perturbation*. Moon's position is based on DE431 Ephemeris model.[7]
- *Atmospheric drag perturbation on flat surfaces*. The atmosphere density is based on Jacchia-Roberts model. Solar activity coefficients (F107-AP index) are available from NOAA Solar flux prediction model-2016 update.[8–10]
- *Solar radiation pressure on flat surfaces*. Solar activity is taken into account and the solar coefficients (F107-AP index) are available from NOAA Solar flux prediction model-2016 update.[10]

The propagation is performed using a Runge–Kutta–Fehlberg 7(8) method on a *C* compiled code.

2 Orbital Injection Strategies

The orbital injection of nanosatellites is crucial in determining the subsequent natural orbital evolution, since the lack of orbit control capabilities. In particular, the relative natural dynamics between the satellites of a constellation is specifically dependent from the orbital injection phase. In general, the relative positions of the spacecraft are not fixed in time. Thus the constellation design has to optimize this dynamical evolution of the uncontrolled relative orbits, coping with differential environmental perturbations, orbit acquisition inaccuracies, and limitation in the launch options availability.

This aspect is particularly relevant for HERMES constellation design, which has to guarantee a minimum physical baseline between the satellites. The proposed solution for HERMES mission can be applied to a generic constellation of nanosatellites without on-board propulsion subsystem. The aim is to propose a smart solution to a typical nanosatellite mission limitation. In particular, this section presents a discussion on the solutions to naturally bound and passively control the relative motion of different nanosatellites injected in low Earth orbit.

Two main options are possible to achieve a non-null relative distance between the satellites as follows.

- Dedicated multiple injections—one per satellite—into different true anomalies at t_0.

- Single injection of multiple spacecraft with initial relative motion imposed by the deployer's release spring. In this case, it is convenient to release the satellites in groups of three elements (i.e., triplets), imposing a certain relative dynamics to each triplet.

The first option is highly sensitive to the release conditions: natural perturbations provoke a slightly controlled relative drift, which is emphasized by the launcher and deployer injection uncertainties. Moreover, this option asks for a dedicated launch, making it less convenient, especially for nanosatellites.

The second option can be realized even if no dedicated launch is settled. A triplet can be released in a single launch event with no dedicated maneuvers. N satellites are released with $N/3$ single injections. The shift in true anomaly between different triplets' release events is settled at design level and it is affordable by either a single launcher maneuver or with separate launchers. Furthermore, the relative motion is actually imposed by the deployer spring authority, which overcomes the natural perturbations effects and the launcher injection uncertainties, as will be discussed in Sec. 5.2. Hence, the expected scientific outcomes are more robust with respect to the release conditions.

A formation-flying-like triplet scenario would be beneficial to keep the spacecraft within acceptable bounded motion throughout the mission. Nevertheless, the lack of propulsion, the launcher inaccuracies, and the spring injection Δv prevent the bounded motion to be achieved.

2.1 *Dedicated Multiple Injections*

In the case of dedicated multiple injections, the initial true anomaly separation yields differential perturbation acceleration resulting in a secular drift of the satellites. Formation flying and, in general, distributed space systems orbital design often relies on linearized, unperturbed dynamical models given the short relative distances acquired, and maintained during the mission. HERMES spacecraft are rather peculiar because of the large distances involved, which are reached during the mission, coupled with the incapability to perform orbit control. The relative motion is hence unbounded, but it is quasiperiodic. Given the importance of their relative motion, it is critical to assess the influence of perturbations, initial true anomaly, and spring injection, on the long-term orbital motion. In case Keplerian motion is considered, the relative positions of the satellites are easily predicted throughout the whole mission. In addition, the relative positions are invariant to the initial true anomaly separation. Obviously, in reality, this is not the case due to the irregular shape of the Earth, leading to differential perturbations. Natural motion due to spherical harmonics is highly dependent on the initial true anomaly of the three satellites. Figure 1 shows the orbital acceleration, as a function of the satellite true anomaly, with gravitational perturbations up to J_{22}, along a 550-km nearly equatorial orbit.

The acceleration components are represented in the local-vertical/local-horizontal (LVLH) frame, which is defined by the radial vector pointing outward (i.e., zenith direction) and by the orbital angular momentum. The third axis completes the right-handed triad, in the horizontal direction with respect to the ground. The latter component is oriented in a direction very close to the along-track direction (i.e., velocity). Note that for circular orbits, the horizontal component is parallel to the velocity direction.

A differential value in the along-track acceleration component, shown in Fig. 1(b), builds up a non-null relative velocity, which yields disparity in the accumulated orbital motion. This differential effect is highly dependent on the initial true anomaly of the satellites, resulting in a non-static relative motion that is hardly predictable during the design phase, because of inherent uncertainties on $\theta(t_0)$. In fact, true anomaly precise injection is hardly achievable in typical nanosatellite launch and deployment phases. Moreover, it may be noted how the periodicity of the perturbation acceleration in the horizontal direction is $>2\pi$ [see Fig. 1(b)]. This is due to the physical source of the perturbation, which is the Earth geopotential. Hence, the period of the resultant acceleration is the revisit time of Earth location, rather than orbital period with respect to the inertial frame. Indeed, it is possible to quantify the angular displacement, after one orbit, of these two reference frames as ~ 24 deg, for the considered 550-km nearly equatorial orbit.

The perturbation accelerations are several orders of magnitude lower than the dominant Keplerian dynamics, as shown in Fig. 2. The Keplerian acceleration power spectral density

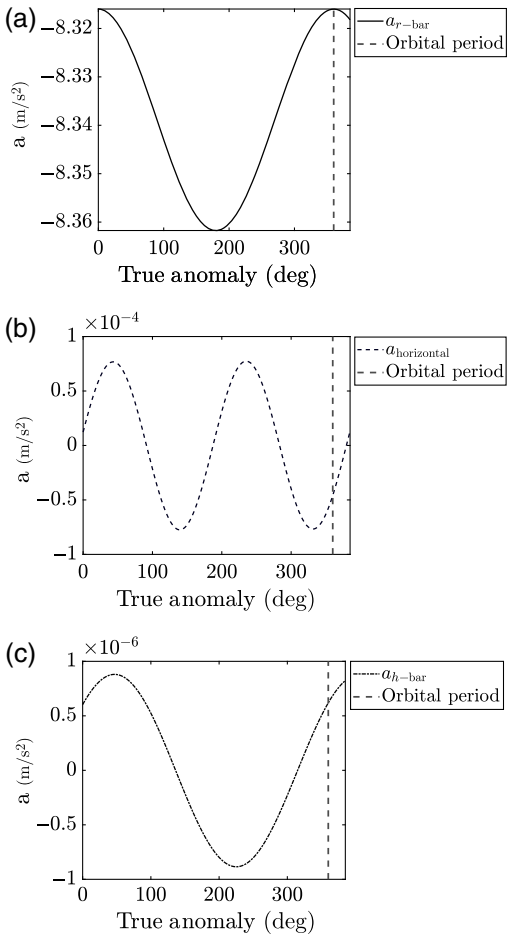

Fig. 1 Orbital acceleration, with gravitational harmonics up to J_{22}, on a 550-km nearly equatorial orbit, expressed in LVLH frame. (a) Radial direction component, (b) horizontal direction component, and (c) orbital angular momentum direction component.

(PSD), reported in Fig. 2(a), refers to the osculating orbit point-wise two-body acceleration. Being osculating orbits, beside the frequency peak corresponding to the orbital motion, the PSD shows a small peak at twice the frequency, which is linked to the periodicity of magnitude of the radius of the osculating orbital motion. The gravitational perturbation acceleration PSD, in Fig. 2(b), shows the peaks corresponding to the orbital mean motion and its integer multiple due to the spherical harmonic terms. The accumulated differential velocity with initial true anomaly separation of 20 deg is in the order of 5 to 10 m/s, according to the acceleration field analysis up to J_{22}.

This result prevents the multiple dedicated injections from being a good option, beside the fact of increasing the cost for dedicated launches or launcher phasing maneuvers. Even for multiple dedicated launches, the nanosatellites deployment is performed using a preloaded spring, which injects the spacecraft into orbit. In order to inject a spacecraft at a defined true anomaly (e.g., the case of multiple injections), the natural motion is exploited. In particular, a harmonic motion cross track is pursued to keep the satellite around a specific true anomaly, vanishing the effects of the initial spring Δv. In this case, gravitational perturbations drive the natural motion. This technique is valid for any nanosatellite injection. Indeed, since the spring release impulse is inevitable, one smart solution to maintain a given true anomaly without drifting is to be injected across track.

2.2 *Single Injection of Multiple Spacecraft*

In the case of single injection, the relative motion could be restrained to bounded relative orbits only if along-track injection Δv is null. Such condition would be beneficial with respect to the

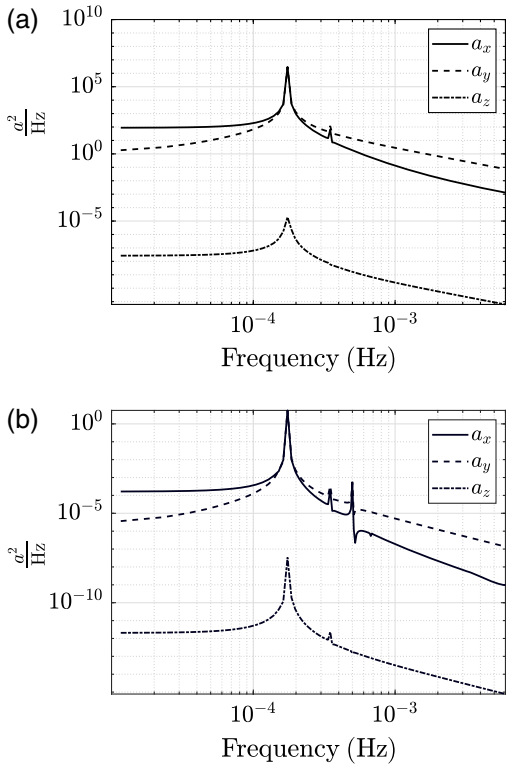

Fig. 2 PSD of orbital acceleration on a 550-km nearly equatorial orbit, expressed in inertial frame. The PSD frequency range is shown within the validity of Nyquist–Shannon sampling theorem, with reference to the data-set sample time (i.e., 60 s). (a) Keplerian acceleration and (b) gravitational perturbation acceleration up to J_{22}.

temporal evolution of the relative distances between the satellites, but several considerations need to be made if a single-injection strategy is analyzed. As said, a bounded relative motion can be achieved by vanishing the along-track differential velocity. Such method relies on the energy-matching principle, in which the energy of the absolute orbits of the different spacecraft are equal.[11,12] An impulse on the radial-cross plane results in a bounded motion. Nevertheless, the entity of the Δv provided by the spring is not enough to inject the spacecraft into three different orbits that result in a bounded relative motion respecting the minimum required mutual distance. Figure 3 shows the maximum achievable distance during bounded cross-radial motion as a function of the injection angle in the radial-cross plane. The maximum reachable relative distance is in the order of 10^1 km, which is far from being acceptable for the imposed scientific requirement of 10^3 km. This sets the need to introduce a relative unbounded drift between the satellites to achieve, at least for a certain amount of time, the required baseline. Indeed, inserting a relative drift makes the formation loose with a periodic relative motion. The satellites need to be injected into different directions to prevent two, or more, satellites from being too close during mission operations. A satisfactory strategy consists in injecting the three satellites along $+v$, $-v$, h-bar, respectively; the injection condition is expressed in the LVLH frame of the launcher at injection time. The satellites injected along-track start drifting, whereas the spacecraft injected cross track evolves in a harmonic motion around the injection point. In this condition, the resultant relative motion propagated for $\sim$3 days is depicted in Fig. 4.

In a realistic scenario, a true simultaneous injection is hardly feasible. However, the above considerations have been proven to be still valid when dealing with short-delayed injections ($\sim 10/15$ min). The nanosatellites deployment is performed also in this situation using a preloaded spring, which injects the spacecraft into orbit. The analysis on the long-term perturbed propagation has shown that spring release injections with at least 0.25 m/s dominate the relative dynamics imposed by the natural perturbations, as presented in Sec. 5. Hence, the design can be done regardless of the initial injection true anomaly, as will be discussed in what follows in this paper.

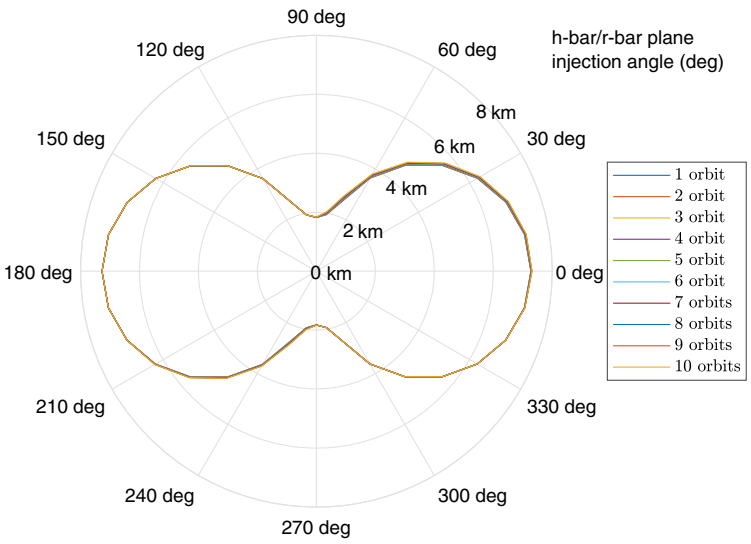

Fig. 3 Maximum achievable distance during bounded cross-radial motion as a function of the injection angle with a spring $\Delta v = 2$ m/s.

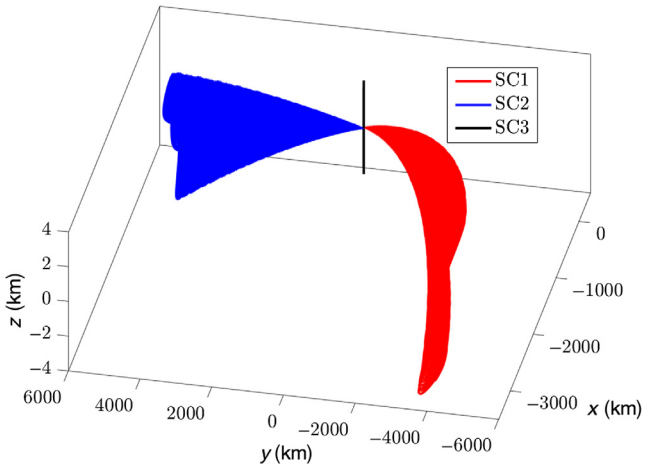

Fig. 4 Injection strategies forcing relative drift to quickly achieve the required relative distance. The satellites are injected along $+v$, $-v$, h-bar with a spring of $\Delta v = 2$ m/s. The physical baseline is achieved in ~3 days.

3 Methods for Sky Visibility Evaluation

The HERMES constellation sky visibility depends on the pointing direction of the satellite's FOV. In fact, despite the orbital control is not available and the positions of the spacecraft are completely dependent from the imposed natural motion, the attitude control is accessible to align the scientific instruments on different regions of the sky, allowing the overlapping of at least three satellites' FOVs. In particular, the accurate selection, alignment, and maintenance of certain pointing directions can be exploited to enhance the whole mission scientific return, by increasing the time and the area of the sky that can be used to perform GRBs triangulation.

The resulting performance index for the constellation is defined as an area of the sky that can be viewed by at least three satellites for a certain amount of time and, thus, is denoted as time-area parameter: tA, whose dimensional units are steradians-day (sr-d). Time-area parameter is defined so to be well suited to estimate the number of expected GRBs detected by the HERMES constellation. In fact, according to previous missions, the rate of measurable GRBs is known. For example, FERMI-GBM[13,14] mission detects ~250 GRB per year in the whole sky not

covered by the Earth (i.e., ~ 8 sr), which corresponds to almost 1 GRB every 1.5 days in the FOV of ~ 8 sr, or 0.083 GRB/sr-d.

3.1 *Sky Visibility Tool*

The evaluation of the performance time-area parameter is performed with a sky visibility tool developed and validated by the authors at Politecnico di Milano.

The visibility tool takes as input the trajectory parameters of the N satellites. It propagates the orbital dynamics with the orbital propagator described in Sec. 1.2 and evaluates the time-area performance parameter. The developed tool, which is extensively used for HERMES mission analysis, is actually a generic framework that can provide useful insights for any mission that includes visibility optimization and pointing constraints. In addition, it is foreseen to be employed during operations planning. The optimized pointing can be predicted in the short time horizon using in-flight orbital data.

3.1.1 *Satellite position constraints*

The software implements the scientific requirement and constraints, as well as possible system and platform constraints. At each iteration steps, the tool verifies if the satellites position with respect to the Earth surface is compatible with the observations. For example, large radiation flux regions are not compatible with scientific instrument operations, as high-leakage currents in the active detectors may damage the payload. Similarly, when the satellites are in eclipse regions or ground stations areas, they may be not able to correctly observe the sky for power or antenna orientation constraints. For this reason, position requirements are enforced at all times for any i'th satellite S_i as

$$S_i \in \mathcal{A} \Leftrightarrow \mathbf{r}_i \in \mathcal{P}, \tag{1}$$

where $\mathcal{A}$ is the set of active satellites, $\mathbf{r}_i$ is the position vector of S_i, and $\mathcal{P}$ is the set of allowed positions. For example, Fig. 5 shows the allowable regions in black with respect to the radiation flux constraint. In general, any constraints on the scientific operations of a nanosatellite dependent from the orbital position can be implemented in a similar way.

3.1.2 *Satellite FOV*

The FOV of the satellite is characterized by the specific instrument installed on-board. It can be defined as a region of the sky that is enclosed within certain geometrical boundaries. In HERMES, the instrument's FOV is the semisphere in front of the detector plane. However, the

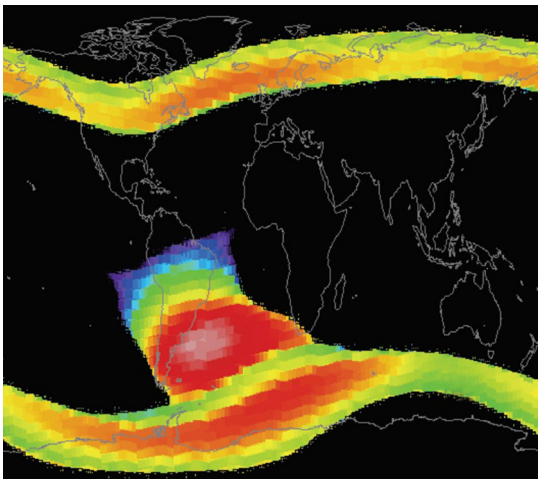

Fig. 5 Large radiation flux regions. Allowed positions in black.

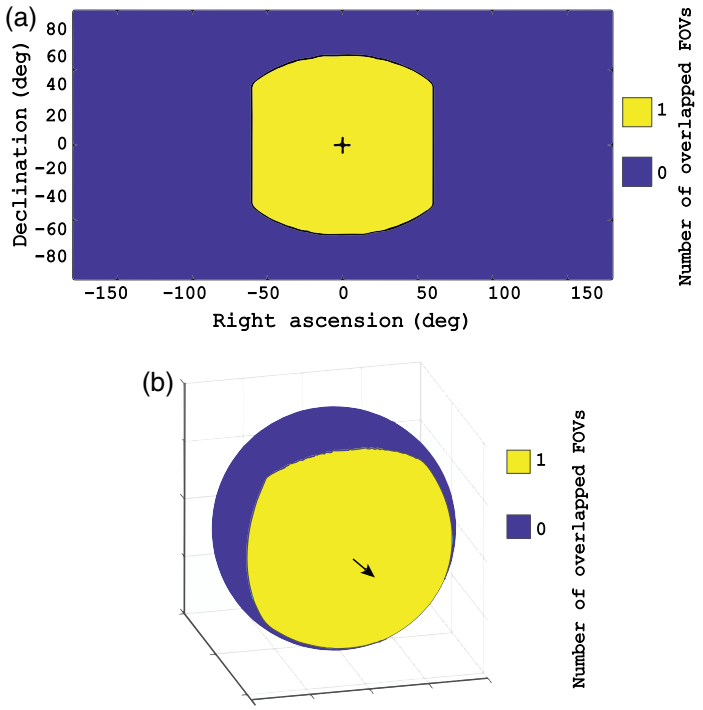

Fig. 6 Single instrument FOV. Pointing direction $\hat{\mathbf{p}}$ in RA $= 0$ deg and DEC $= 0$ deg. (a) 2D projection and (b) 3D view.

sensitivity of the detector has a cosine profile with respect to the line of sight (LOS) and, thus the full-width at half-maximum of the instrument is 120 deg. As a consequence, for each active satellite, the effective FOV is defined as the portion of the celestial sphere with an angular distance <60 deg with respect to the instrument axial planes, Π_x and Π_y, as reported in Fig. 6. In particular, for a given pointing direction of the LOS of the instrument $\hat{\mathbf{p}}$, which is found by the intersection of the two axial planes as

$$\hat{\mathbf{p}} = \Pi_x \cap \Pi_y, \tag{2}$$

the FOV of the i'th satellite $\mathcal{F}_i$ is defined as

$$\mathcal{F}_i = \left\{ \hat{\mathbf{s}} \middle| \left(\hat{\mathbf{s}} \angle \Pi_x \leq \frac{\pi}{3} \right) \wedge \left(\hat{\mathbf{s}} \angle \Pi_y \leq \frac{\pi}{3} \right) \right\}, \tag{3}$$

where $\hat{\mathbf{s}}$ is a generic direction in the sky.

3.1.3 *Satellite pointing constraints*

The developed tool is capable to include pointing constraints, in order to accommodate possible scientific requirements penalizing certain regions of the sky where the scientific performances are not acceptable. The pointing constraints are divided in "soft" and "hard" depending on the consequences of constraint violations. On the one hand, the soft pointing constraints identify regions of the sky where the satellite could, in principle, be pointing but without yielding valuable scientific measurements (e.g., high instrument noise). On the other hand, hard pointing constraints identify forbidden regions to be pointed, due to the potential degradation of the scientific instrument if not respected. Both constraints are assumed to be always respected, thanks to the attitude control system of the nanosatellite.[15] The soft pointing constraint region is formalized for a given constraint direction $\hat{\mathbf{c}}$ as

$$\mathcal{C} = \{ \hat{\mathbf{s}} | \cos^{-1}(\hat{\mathbf{s}} \cdot \hat{\mathbf{c}}) \leq \alpha_c \}, \tag{4}$$

where α_c is the exclusion angle. Then the effective i'th FOV simply results from

$$\mathcal{F}_{E_i} = \mathcal{F}_i / \mathcal{F}_i \cap \mathcal{C}. \tag{5}$$

It shall be noted that only active satellites belonging to $\mathcal{A}$ have an effective FOV. For satellites that are not active, it results in

$$\mathcal{F}_{E_i} | (S_i \notin \mathcal{A}) = \varnothing. \tag{6}$$

3.1.4 *Triangulable field of view*

According to the imposed scientific requirements, a region of the sky can be triangulated if it is contained in the FOV of at least three satellites. Hence, the overlap of at least three effective FOVs is defined a j'th triangulable FOV as

$$\mathcal{F}_{T_j} = \mathcal{F}_{E_1} \cap \mathcal{F}_{E_2} \ldots \cap \mathcal{F}_{E_i} \ldots \cap \mathcal{F}_{E_N} \quad \text{with } N \geq 3. \tag{7}$$

Figure 7 shows an overlapping map in which six satellites are active at a given epoch. The triangulable FOVs are the yellow regions in the map.

3.1.5 *Baseline requirements*

The physical and the projected baselines for all the possible triangulable regions are evaluated. Indeed, for any j'th triangulable FOV there exist at least three co-observing active satellites, whose physical baselines are immediately available from their orbital position. The projected baselines are computed knowing the pointing directions of each element. If the baseline requirements, described in Sec. 1.1, are satisfied, the triangulable FOV region is kept in the computation. Otherwise, the triangulable region is cancelled and set equal to zero.

3.1.6 *Constellation field of view*

At any epoch, each point in the sky visible by at least one active triplet (i.e., $\mathcal{F}_{T_j} \neq \varnothing$) is considered as observable and triangulable; the total area observed at any time is computed by integrating the observable points over the whole celestial sphere and it is denoted as constellation FOV. The constellation FOV results from the union of all the triangulable FOVs respecting the baseline requirements as

$$\mathcal{F}_C = \mathcal{F}_{T_1} \cup \mathcal{F}_{T_2} \ldots \cup \mathcal{F}_{T_i} \ldots \cup \mathcal{F}_{T_M} \quad \text{with } M \geq 1. \tag{8}$$

The constellation FOV area is measured in steradians (sr). Figure 8 shows the constellation FOV for the considered example.

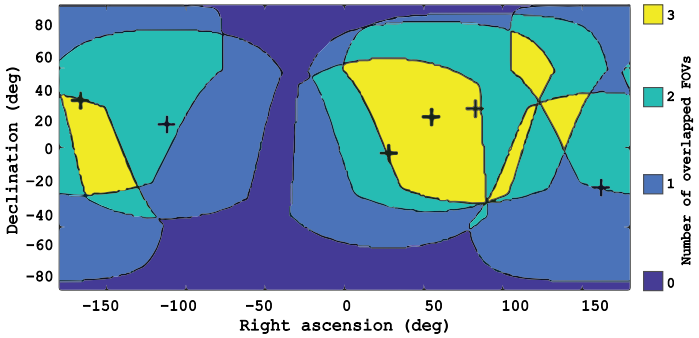

Fig. 7 Satellite FOVs overlap.

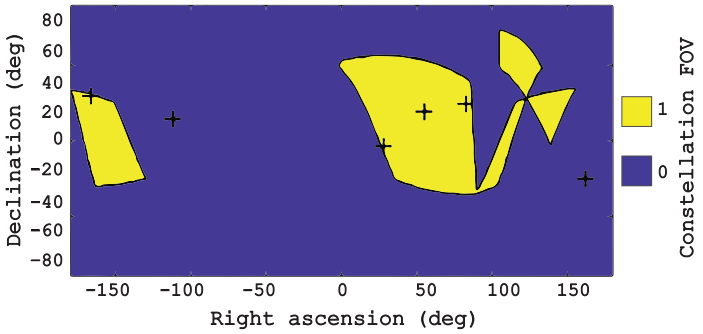

Fig. 8 Constellation FOV.

3.1.7 *Time-area parameter and estimate of observable GRBs*

The instantaneous observable area (i.e., the constellation FOV) is integrated over the whole mission lifetime to obtain the time-area parameter tA. The estimate of the observable GRBs is performed as detailed in Sec. 3.

4 Definition of Operational Pointing Directions

The definition of the pointing directions of each spacecraft, together with their evolution in time, is fundamental elements in the determination of the scientific performance of the constellation. In fact, pointing strategy design has to find a solution that, while minimizing the number of the required attitude maneuvers and the control effort, allows the coverage of distinct and not obstructed regions of the sky with the overlap of $N > 3$ FOVs. The alignment is performed to guarantee the investigation of the celestial sphere on a certain sky area for a minimum amount of time.

Besides simple pointing strategies, such as zenith and fixed inertial pointing, optimized pointing strategies can be implemented, aiming to determine the pointing directions that maximize the scientific outcome of the mission. In this way, the definition of sequential operational pointing directions comes directly from the sky visibility analyses and it is inherently connected to the scientific return of the mission.

The adoption of time-varying optimized pointing directions is proposed to overcome the limitations given by the lack of orbital control. In fact, the natural relative drift between the elements of the constellation determine a temporal evolution also in the overlap of the FOVs aligned with respect to an LVLH direction, as evident from Fig. 9. Therefore, periodic alignments of the different FOVs are required. Ideally, a continuously aligned strategy would be the best option, but this is not feasible due to the limitations inherent with a small space system. In alternative, alignment of the distinct FOVs on inertial directions could provide a different solution to the same issue. However, inertial directions are periodically covered by the Earth surface, leading to a detriment in scientific performances. Moreover, also in this case, periodic alignments on inertially defined regions of the sky are necessary.

Dedicated optimization algorithms have been developed to define the best set of operational pointing directions according to the configurations of the constellation along its dynamical evolution. The frequency of the attitude maneuvers, needed to vary the pointing directions, is not constant and it can be selected by the constellation designer and operators, according to the available attitude management resources and to the required scientific return. The developed optimization algorithms support the constellation design and the baseline scenario selection. However, their capabilities also will be extensively used during the mission operations as a part of the flight dynamics software to set up the pointing sequence schedule.

Given the topology of the constraints on the sky, a heuristic approach has been adopted for the optimization. Indeed, the constraints on the sky lead to a non-mono-convex domain, which means that the domain is a collection of disjoint sets. The selected algorithm is the MATLAB built-in particle swarm, with a swarm size of 20 elements and a maximum number of iteration

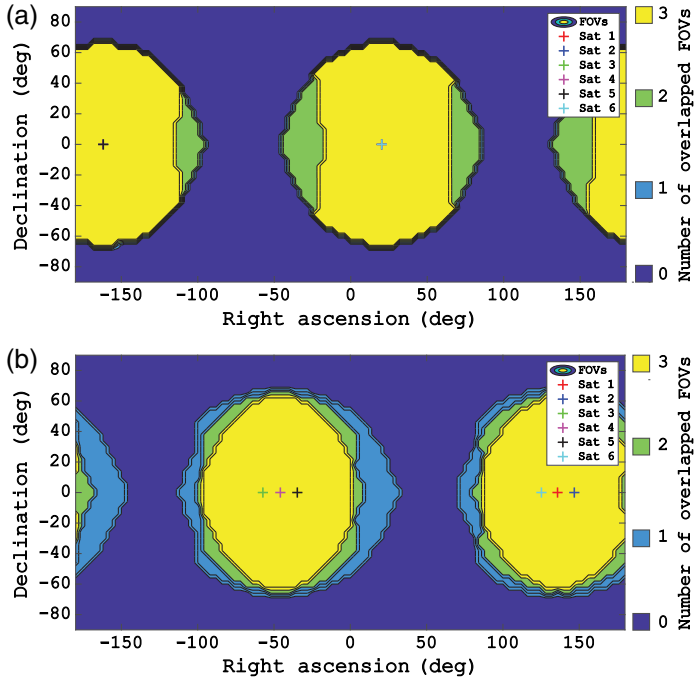

Fig. 9 Constellation FOV evolution along 1 week for a LVLH pointing direction. (a) Constellation FOV at t_0 and (b) constellation FOV at $t_0 + 7$ days.

equal to 100, in order to quickly obtain near-optimal solutions.[16] The best suboptimal solution is then locally optimized using the MATLAB "fmincon" function, which implements an interior-point algorithm to reach the closest local minimum.[17] The numerical effort required to estimate the scientific performances of the constellation with a proper spatial resolution of the sky, using the approach described in Sec. 3.1, is quite computationally intensive. Thus it is very time-consuming to perform the optimization directly on the actual estimate of the triangulated GRBs. Hence, in both optimization algorithms, only a representative subset of the available instantaneous visibility data has been used. This subset includes a finite number of orbital positions of the constellation within the optimization time period, which correspond to different instantaneous drifted sensors positions with the respective constellation FOV configurations.

4.1 *LVLH Optimal*

The working principle of the LVLH optimal strategy is to periodically optimize the direction of the LOS of each satellite with respect to its own rotating LVLH reference frame. As mentioned, it is possible to use a small number of instantaneous visibility data points to estimate with enough precision the effectiveness of a given pointing configuration over a short period (e.g., few days for 1-week optimization). This feature, which reduces the computational time, is beneficial for the integration of such optimized tool in the flight dynamics software for operation planning. Indeed, due to the slow behavior of the relative dynamics between satellites, which is in the order of 80 to 100 days, and due to the fact that the Earth is fixed in the LVLH frame, the constellation FOV evolution is slow and it is not dependent from the orbital positions of the spacecraft. Figure 9 shows the evolution of the constellation FOV along 1 week of simulation, from a generic t_0 to $t_0 + 7$ days. It can be noted how the instantaneous observed area of the sky has little differences, and the only significant time evolution of the FOV is contained in the orbital plane of the spacecraft with a fast periodicity of 2π scan every one orbit.

In order to efficiently exploit this reduction of the optimization computational costs, it is convenient to remove, during the estimation of the triangulable GRBs, the constraints related to the ground track of the satellites (e.g., large radiations flux regions). Indeed, the dynamics of

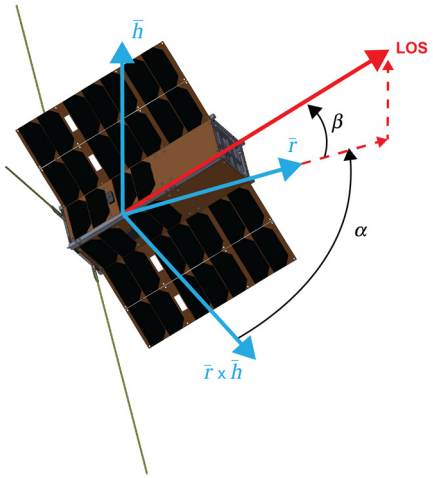

Fig. 10 LOS definition in LVLH reference frame.

this constraint is too fast to be correctly identified and to become part of the optimization process. Moreover, the passages of the satellites in forbidden regions are only barely influenced by the pointing direction.

With more details on the presented example cases, the algorithm takes into account three points for each optimization window (i.e., the first, the median and the last point of each optimization period) and computes the mean triangulated fraction of the sky. It uses two angles for each satellite, α and β in Fig. 10, as optimization variables to define every LOS in the LVLH frame during the optimization time window. Therefore, for 6 satellites, 12 optimization degrees of freedom are exploited. The optimization algorithm employs 5 to 15 s for each optimization period, depending on the satellite configuration, on a 2.6-GHz Intel i7 processor, with no parallel computing technique.

It is interesting to underline that this pointing strategy includes also one particular solution, in which all the spacecraft are zenith pointing. Nevertheless, this is typically not the optimal one, since a beneficial overlap of the spacecraft fields of view is not possible when the spacecraft have enough physical baseline.

4.2 *Inertial Optimal*

The working principle of the inertial optimal strategy is to periodically optimize the direction of the LOS of each satellite with respect to the inertial reference frame. Different from the strategy presented in Sec. 4, the Earth is moving with respect to the FOV of each satellite with a period of one orbit (i.e., ~90 min). Therefore, the dynamics of the constraints is not slow enough to allow the optimization on a reduced set of equally spaced data, as in the LVLH optimal case. Anyway, the relative orbital dynamics between satellites is not correlated with the pointing strategy and thus shows the same slow dynamics presented in Sec. 4. In order to match both the fast and the slow dynamics of the constraints, the optimization of the LOS direction of each satellite is performed using a more refined time grid over one orbit (e.g., 18 points in one orbit, for the presented example cases).

The logic of the optimization algorithm is similar to the one presented before, with the difference that the optimization variables α and β are defined with respect to the inertial reference frame, and the number of points in the optimization window is larger. The optimization algorithm requires 20 to 50 s for each optimization period, depending on the satellite configuration, on a 2.6-GHz Intel i7 processor, with no parallel computing technique. The advantage of the inertial optimal solution is related to the possibility to easily implement and satisfy pointing direction requirements or constraints on the sky. The pointing requirements or constraints are typically limiting static inertial regions of the celestial sphere, which, in turn, are time varying if projected in the LVLH frame.

4.3 *Influence on Astrophysical Data Return*

The two different optimized operational pointing strategies have a direct influence on the astrophysical data return in terms of accuracy of the triangulation, coverage of the sky regions, and number of triangulated GRBs. The latter is also influenced by the frequency of pointing directions variation, related to the number of necessary attitude maneuvers, which is also discussed in this section.

Triangulation accuracy is related to the baseline value of the observations. In fact, even if the required minimum baseline is 1000 km, the larger is the projected baseline value during triangulation, the better is the accuracy of the measurements. Figure 11 shows the statistical distribution of the triangulated GRBs as a function of the projected baseline for the LVLH pointing strategy. Since most of the GRBs are observed with a baseline between 1000 and 5000 km, which is larger than the required one, this pointing strategy leads to a good accuracy in locating the astrophysical events in the celestial sphere. Figure 12 shows the statistical distribution of the triangulated GRBs as a function of the projected baseline for the inertial optimal pointing strategy. The typical value for the observation baseline (i.e., ∼2000 km) is lower with respect to the LVLH optimal pointing strategy. Therefore, the localization of the GRBs in the sky is less accurate for inertial optimal pointing, with respect to the LVLH one.

Figure 13 shows the coverage of the sky for the whole two years mission for both inertial and LVLH-optimal pointing strategies on equatorial orbits. The adoption of different pointing strategies leads to different coverage of the sky: while the inertial pointing strategy promotes the

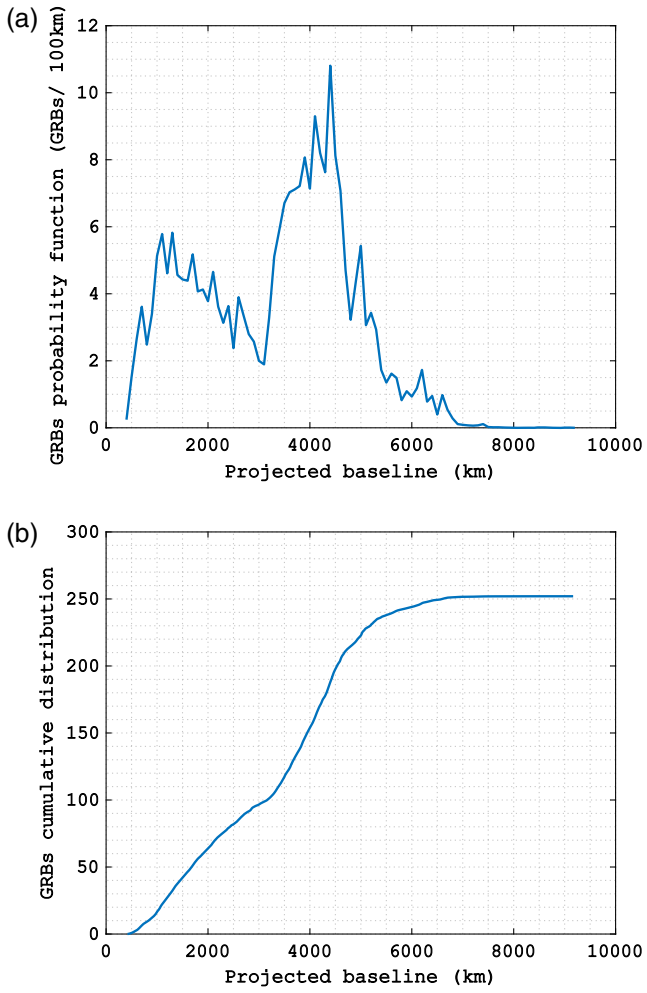

Fig. 11 Projected baseline distribution for LVLH optimal pointing triangulation: (a) Probability density function and (b) cumulative density function.

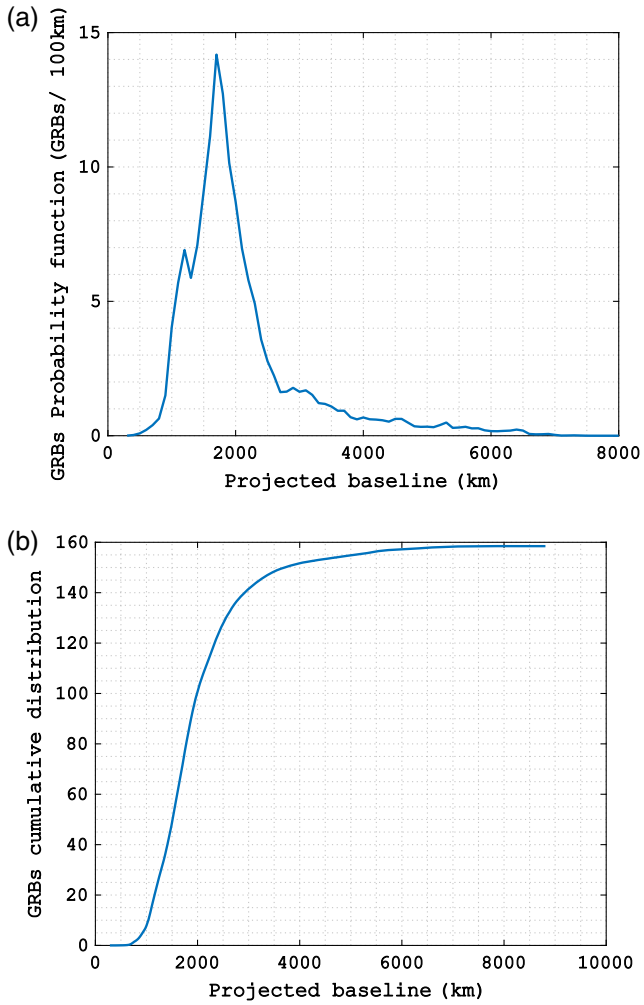

Fig. 12 Projected baseline distribution for inertial optimal pointing triangulation: (a) probability density function and (b) cumulative density function.

visibility of the polar regions, the LVLH-optimal is more suitable to triangulate GRBs in the equatorial region of the celestial sphere, namely from −60 deg to 60 deg of declination. This result highlights how the current design provides a partial analysis of the whole celestial sphere. Hence, to have an investigation over the complete sky catalog, the current constellation design shall be extended, as will be discussed in Sec. 5.3.

The selected pointing strategy has a direct impact also on the raw number of potentially observable astrophysical events. In fact, as evident from Fig. 14, the number of triangulated GRBs is directly dependent from the specific pointing of the constellation. However, the definition of the coordinated LOSs directions is not the only pointing design parameter; the number of alignment attitude maneuvers plays a non-negligible role in determining the scientific output of the mission. In general, since the optimized pointing strategies are evaluated over a certain time window, it is easily arguable how more frequent attitude maneuvers, to periodically align the different FOVs, lead to a finer optimization grid, and thus to better scientific performances. On the contrary, the consequent load on the system platform may be not sustainable within the limitations of a small space system. In these regards, Fig. 14 shows the influence of the maneuvering frequency on the scientific results for both LVLH and inertial pointing. As expected, for both strategies, the higher the optimization frequency is (i.e., lower pointing update period), the better the scientific return is. If the pointing update period is longer than the period of the relative motion (i.e., 80 to 100 days), the two strategies show similar results. In this case, the rare pointing optimization maneuvers do not allow to overcome the limitations due to the natural drift of the constellation. The benefit in selecting specific optimal directions is marginal. Conversely,

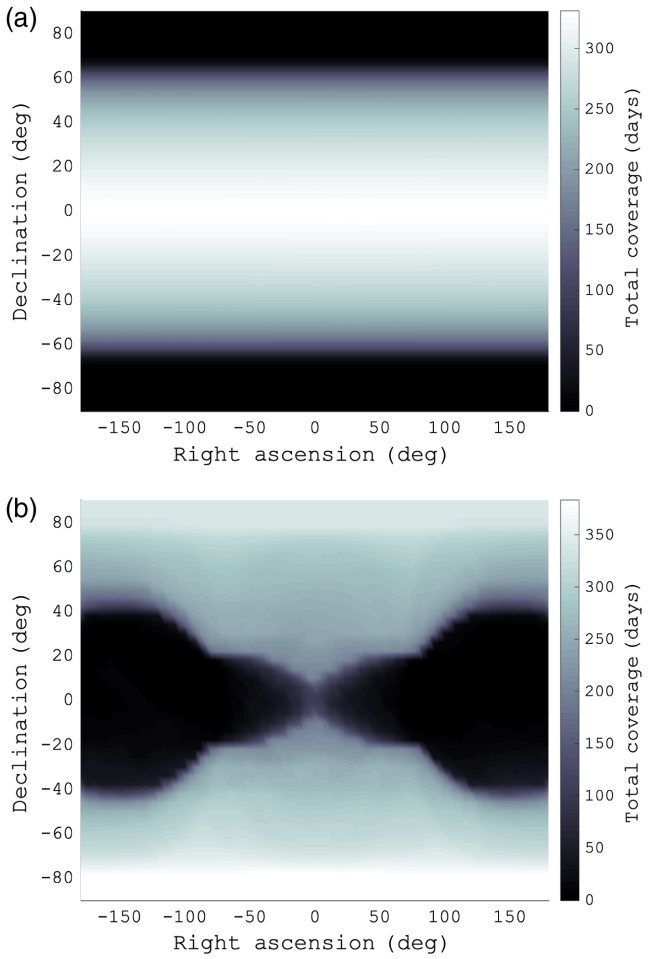

Fig. 13 Sky coverage during the two-year mission on equatorial orbits: (a) LVLH optimal pointing strategy and (b) inertial optimal pointing strategy.

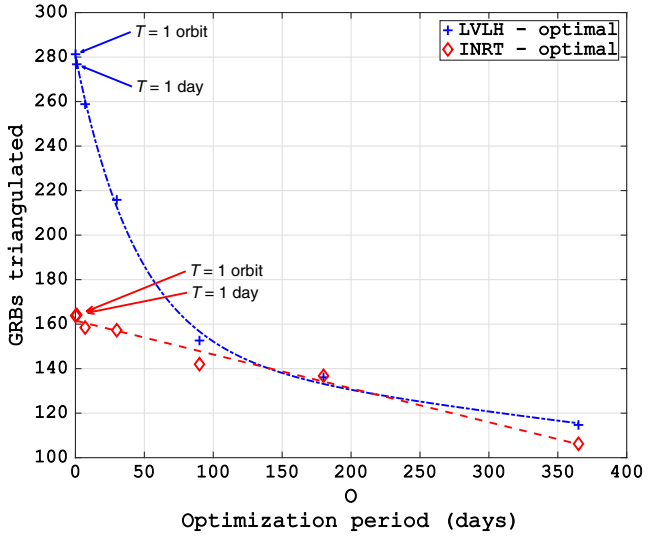

Fig. 14 Influence of the pointing update period on the scientific performances.

if the pointing update period is reduced, the LVLH optimal pointing strategy is able to ensure a higher gain in the number of triangulated GRBs. This strategy beneficially exploits a frequent optimization of the alignment between the constellation elements. In this way, the best FOV overlap is available at any time the satellites are satisfying the position requirements. This is not the case for the inertial optimal strategy since, even with ideal continuous pointing optimization, some areas of the sky are periodically behind the Earth sphere for certain elements of the constellation. Hence, there is an upper limit in the possible scientific gain.

5 HERMES Constellation Scenario

The proposed method has been employed to design and analyze the effectiveness of HERMES constellation. In particular, to consolidate the results with respect to unavoidable injection and release uncertainties, dedicated Monte Carlo statistical simulation campaigns are used.

5.1 *Mission Scenario Definition*

The possible operational orbits, according to the scientific requirements discussed in Sec. 1.1, are nearly equatorial orbits or SSOs with altitude between 450 and 600 km. Due to orbit injection errors, a nominal orbit with altitude of 500 km, or lower, does not guarantee the 2-year mission duration requirement in all the possible cases, with enough confidence. Hence, a nominal orbit altitude of 550 km is selected, in combination of a nominal eccentricity of 0 (i.e., circular orbit). It is worth noting that the presence of large radiation flux regions at the poles of the Earth, as specified in Fig. 5, reduces the available observation time for polar and nearly polar orbits. Indeed, the available estimates of the scientific performances on SSO are tremendously reduced with respect to those on low inclination orbits. Hence, the nominal scenario is set on equatorial orbits with $i = 0$ deg.

For what concerns the injection strategy, the single injection of multiple spacecraft is considered to be favorable both for the greater performances in terms of launcher availability, and for the lower sensitivity with respect to release condition errors, as extensively discussed in Sec. 2. Hence, this is assumed as the nominal injection condition for the considered mission scenario. The remaining free variable is the phasing angle between the releases of the two triplets in the constellation. The nominal angular separation between the two injections of the triplets has been selected with a preliminary analysis on the possible phasing angles between the two release events. In particular, a phasing angle in the order of 140 deg to 220 deg results in better scientific performances. This is because, the central elements of the triplets (i.e., spacecraft injected along the h-bar direction) remain always on opposite side of the orbit, guaranteeing the possibility to

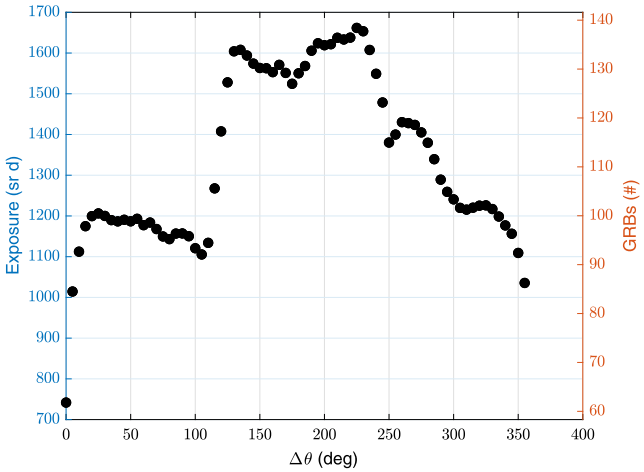

Fig. 15 Estimate of the scientific performances as a function of the phasing angle in the true anomaly separation for two triplets injected at $h = 550$ km. This figure reports both the exposure tA and potentially observable GRBs.

form an active triplet as soon as a third satellite is available with enough relative distance. The triangulable GRBs as a function of the phasing angle between two triplet injections are reported in Fig. 15.

The nominal spring value for the release Δv is selected according to the availability of typical nanosatellite deployers. A nominal release $\Delta v = 1.25$ m/s has been selected. In this case, the relative motion is dominated by the spring authority over the natural gravitational perturbations.

The selection of the nominal optimal pointing strategy is dependent from the comparison in Sec. 4.3 and from the robustness analysis discussed in the next section. An example pointing update period of 1 week is used, being a good compromise between the complexity of the spacecraft operations and the scientific return.

5.2 *Robustness Assessment with Statistical Analysis*

To assess the confidence on the estimate of the scientific performances and the robustness of the proposed mission scenario with respect to unavoidable injection uncertainties, a comprehensive statistical analysis is set up. In particular, a Monte Carlo simulation campaign is used.

The pool of uncertain variables adopted for the robustness analysis is reported in Table 1. The selected set includes launcher's and deployer's injection errors.

As far as the launcher is considered, both temporal and orbital uncertainties are taken into account. In particular, the time variability is represented by a 2-year wide launch window (i.e., the launch date is within 2 years from April 1, 2020) and a 2-day wide phasing window (i.e., the second triplet is released in a different point of the orbit within 48 h from the first triplet). It is worth noting that the phasing window can be extended to a longer time frame without significant changes in the results. The orbital uncertainty of the launch is represented with errors in all the six Keplerian parameters of the nominal orbit. The reference values for launcher injection uncertainties come from the combination of the worst cases among the European launchers (e.g., Vega, Ariane 5, and Soyuz), with a margin of 100%.

In addition, the analysis considers the uncertainties for the release from the deployer. In fact, after each triplet is injected with uncertainties into the orbit, the spring release of each satellite from the deployer is taken into account. The three satellites of each triplet are released in three different LVLH directions to achieve the desired relative motion. The spring release is affected

Table 1 Nominal variables, ranges, and random errors.

	Nominal value	Design range		Random error	
		Range	Distr.	3σ	Distr.
Launcher					
Launch window (year)	0	2	Uniform	—	—
Phasing (h)	0	48	Uniform	—	—
SMA (km)	6928	—	—	30	Normal
e (–)	0	—	—	0.0024	Half-normal
i (deg)	0	—	—	0.30	Normal
ω (deg)	0	—	—	1.2	Normal
Ω (deg)	0	—	—	0.4	Normal
θ (deg)	0 and 220	—	—	1.2	Normal
Release					
Spring Δv (m/s)	1.25	0.25	Uniform	10% of Δv_{nom}	Normal
Injection angle (deg)	0	—	—	4	Normal

by errors in both the magnitude and direction of the spring Δv, as listed in Table 1. The injection angle error is taken from the worst cases among the European launchers in terms of upper stage attitude control accuracy, margined by 100%. For what concerns, the uncertainty on the impulse imposed by the release spring, uniform distribution around the design nominal value of $\Delta v_{\text{nom}} = 1.25$ m/s is used. For each run of the analysis, a unique uniformly dispersed Δv_{run} value is selected within the spring Δv range (i.e., spring value for the single run $\Delta v_{\text{run}} = \Delta v_{\text{nom}} \pm$ uniform). This is done to prove the robustness also with respect to different spring Δvs of commercially available deployers. Then each satellite is released with the actual spring value Δv_{sat}, which is dispersed normally around Δv_{run} (i.e., $\Delta v_{\text{sat}} = \Delta v_{\text{run}} \pm$ normal).

The number of runs of the statistical analysis is selected to represent the global response of the system to the assumed uncertainties, according to Hanson.[18] The goal of the analysis is to estimate the value of the expected triangulable GRBs by the constellation of nanosatellites. Therefore, in terms of statistical analysis, the goal is to estimate the mean value of the expected GRBs and to bound the scientific output within a box at ~99.73% of probability to achieve the scientific result. Preparatory analyses showed that with ~100 samples the standard error of the estimated mean was below 2 GRBs. In this way, the expected mean number of GRBs can be estimated with a precision range of 5. Pool of variables is created exploiting a Mersenne Twister random number generator with seed continuously shuffled according to code execution time on different servers.

The results for the statistical analysis employing the LVLH optimal pointing, described in Sec. 4, are reported in Fig. 16.

At 550-km nominal altitude, the mean value of expected GRBs is 234.80, the standard error of the mean is 1.94, and the standard error of the standard deviation is 1.39, as reported in Table 2. Hence, the mean value of expected GRBs is estimated to be between 228.98 and 240.62 at 99.73%.

The results for the statistical analysis employing the inertial optimal pointing, described in Sec. 4, are reported in Fig. 17.

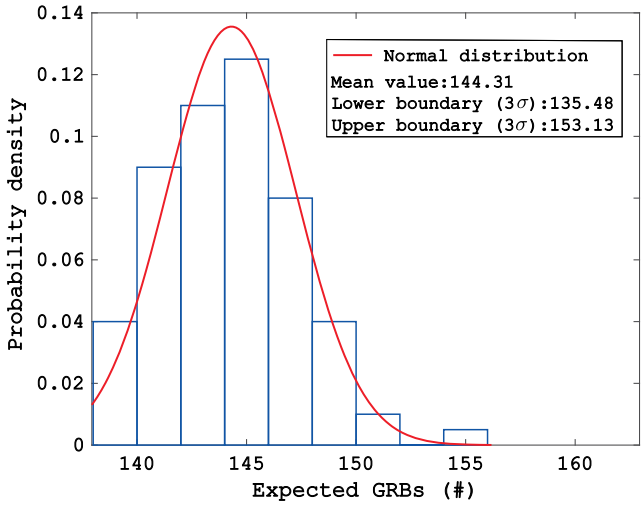

Fig. 16 Statistical analysis results for the optimized LVLH pointing. Number of expected triangulable GRBs throughout the mission.

Table 2 Robustness analysis results for the LVLH optimized pointing strategy.

h (km)	μ (GRB)	3σ (GRB)	SE_μ (GRB)	SE_σ (GRB)
550	234.80	57.03	1.94	1.39

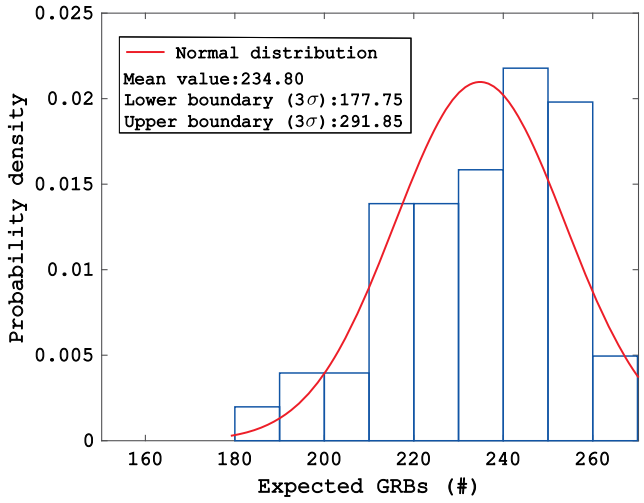

Fig. 17 Statistical analysis results for the optimized inertial pointing. Number of expected triangulable GRBs throughout the mission.

Table 3 Robustness analysis results for the inertial optimal pointing strategy.

h (km)	μ (GRB)	3σ (GRB)	SE_μ (GRB)	SE_σ (GRB)
550	144.31	8.83	0.30	0.22

At 550-km nominal altitude, the mean value of expected GRBs is 144.31, the standard error of the mean is 0.30, and the standard error of the standard deviation is 0.22. Hence, the mean value is estimated to be between 143.41 and 145.21 at 99.73%, as reported in Table 3.

The statistical analysis presented in this section has been used to prove that the estimate of triangulable GRBs is basically uncorrelated to the uncertain variables taken into account in the mission analysis. This feature is beneficial in terms of mission design, given that the statistical analysis was performed against typical launch and injection uncertainties. Thus the presented statistical analysis does not explore different mission concepts (e.g., correlation with design variable), rather it guarantees the achievement of nominal results.

The LVLH optimal pointing strategy is confirmed to provide better results than the inertial optimal one, in terms of both number of triangulated GRBs and typical observation baseline. One reason for such result is the FOV occultation due to Earth. In the inertial pointing, Earth enters the FOV of the satellite instruments forming a triplet, alternately. This leads to preferred pointing regions close to the poles, which in turns are restricted by the achievable projected baseline. This degrades the performance in terms of available observation time and observable regions. The lower standard deviation of the inertial distribution may be due to the modest sensitivity to relative motion, differently from the LVLH pointing strategy, which has a temporal drift in the FOV overlap, as discussed in Sec. 4. For the aforementioned reasons, the nominal pointing strategy for the HERMES mission scenario described in Sec. 5.1 is the LVLH optimal.

As anticipated in the description of the mission scenario, the correlation of deployer spring Δv with the scientific outcome has been assessed with a Monte Carlo campaign on a set of 250 samples. In particular, weak correlations are outlined in Fig. 18. The Pearson's linear correlation coefficient is 0.43. In addition, it is here remarked that, as the Δv decreases, the dispersion of the expected GRBs increases, and the absolute number decreases. This may be explained by the fact that, for low spring impulses, the relative motion is governed by the differential geopotential acceleration experienced at injection into orbit; hence it is highly sensitive to initial conditions. On the other hand, the relative motion is governed by the imposed impulse whenever higher Δv is delivered by the spring.

The robustness of the mission design is sought also with respect to non-nominal configuration scenarios and eventual satellite failures. One potential non-nominal configuration is the

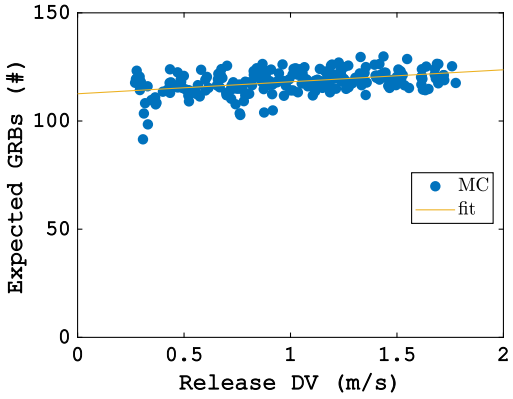

Fig. 18 Correlation between potentially observable GRBs and release spring Δv.

presence of a single triplet. Results show that acceptable scientific outcome can be guaranteed even with just three satellites, scaling almost linearly the number of expected GRBs regardless of the operational pointing strategy (i.e., ∼50% scientific performances reduction with respect to a constellation of six elements). The analysis is useful to evaluate a hypothetical scenario, in which the two triplets are launched with a significant in between delay. Indeed, in such configuration, the six satellites constellation would exist far <2 years. For instance, assuming the two triplets are launched 1 year apart, the constellation will function as a single triplet for 1 year, a six satellites constellation for another year and, again, as a single triplet for the last year. A further possible non-nominal configuration is a five satellites constellation. This is representative of an early failure in a single space element (e.g., one satellite is lost during injection or commissioning phase). The results demonstrate that losing the possibility to form two distinct triplets reduces the performances to almost those available with a single triplet. In fact, at any instant of time, the constellation FOV is analogous to the one available with just three elements. However, five satellites have better performances than a single triplet. This is because five satellites reduce the time, in which triangulation is not possible due to position constraint violation of a single element in the constellation. Thus a satisfactory robustness toward a single satellite failure is present. Indeed, the reduction in the estimate of the scientific performances is in the order of ∼40%, with respect to a constellation of six elements, for both operational pointing strategies.

5.3 *Extension to a Full Constellation*

The present mission design is dedicated to the improvement of the scientific performances within the HERMES pathfinder mission requirements. However, the constellation configuration can be extended to achieve better or more astrophysical data. In fact, the major shortcoming of the current design is the limitation in having all the spacecraft on a single orbital plane. This is motivated by the launch opportunity availability, but does not allow a complete three-dimensional triangulation. In fact, the hemispherical uncertainty, with respect to astrophysical events coming from above or below the orbital plane, cannot be solved by the proposed configuration. Moreover, the selection of the LVLH optimal pointing strategy leads to an incomplete catalog of observable astrophysical events, restricted to those coming from the equatorial section of the celestial sphere, as outlined in Sec. 4.3.

A complete sky coverage can be achieved by dividing the two triplets, in a way that one is inertial pointing and, the other, LVLH pointing. Nevertheless, a lower number of triangulated GRBs are expected. It shall be noted that an increase in the frequency of pointing updates, even with a mix of inertial and LVLH directions, does not solve the intrinsic limitations of the present configuration. Additionally, it may overstress the attitude control subsystem, potentially leading to premature failures of the small space system. Then the simple enlargement of the constellation in its current configuration is not the best viable solution.

The proposed extension to an FC of small satellites for localization and triangulation of astrophysical events is to have $N_{SC} > 6$ spacecraft, subdivided in different orbital planes. The greater part of the constellation shall be located at low inclination (i.e., ≤30 deg, while few

complementary triplets shall be placed in nearly polar orbits. This design would allow a complete sky coverage, with the possibility to completely solve the three-dimensional localization of the astrophysical event. With this configuration, all the spacecraft can be pointed in LVLH optimal directions, guaranteeing a positive scientific return, and solving the limitations of the pathfinder design.

The specific values of the scientific performances for the FC composed of N_{SC} satellites, along a 2-year mission, are: $\geq$15 GRB/SC for zenith pointing without optimization maneuvers, and $\geq$35 GRB/SC for LVLH optimal with update period of 1 week. The lower bound of the specific performances for the FC is relative to $N_{SC} = 18$, whereas a smaller constellation typically guarantees better specific values.

6 Conclusion

This paper introduced a general framework for the mission analysis and sky visibility evaluation of distributed instruments flying in nanosatellites constellation. The study case was applied to the HERMES constellation, dedicated to the detection and localization of high-energy astrophysical transients. In particular, the propulsion-less nature of the mission forced an accurate and detailed analysis of the dynamical behavior of the satellites in natural motion. The definition of constellation injection strategies to assure the fulfillment of scientific requirements was presented. This analysis was supported by a thorough investigation on the influence of the injection impulse, as well as the most significant gravitational field perturbations.

In order to overcome the limitations given by the lack of orbital control, resulting in a temporal drift of the constellation, specific pointing strategies for the scientific instruments were discussed. In particular, an optimization routine was proposed to increase the scientific return of the mission, computing the most-performing pointing directions for the coordinated satellites. The available pointing strategies were compared and critically discussed with respect to their influence on astrophysical data return, in terms of accuracy of the localization, coverage of the sky regions, and the number of observed events.

The resulting constellation baseline entails a quasisimultaneous injection for multiple spacecraft along three different directions, namely $+h$, $+v$, and $-v$-bar. Such strategy guarantees a relative natural drift that ultimately takes the satellites to the required physical baseline. The pointing strategy is optimized with respect to LVLH pointing directions. A comprehensive mission analysis tool, coupled with a high-fidelity dynamical propagator, was developed to assess the scientific performance of the constellation, taking into account all the imposed mission requirements. The available simulated results were used to support the presented discussions, assess the robustness of the proposed design and propose possible extension to an FC.

The simulation set-up and the proposed methodology can be easily extended to include any constraint, expressed with the same mathematical formulation. This allows the tool to be implemented for different mission scenarios, involving distributed instrumentation in propulsion-less nanosatellites constellations. In addition, the methodology can be applied to Earth-monitoring and planetary remote sensing constellations, in which the pointing direction and FOV calculation are simply transferred to Earth or planet projections. The proposed analytical and optimization technique can easily include ground related scientific merit parameters, as long as they can be defined with mathematical sets and formulas.

Acknowledgments

The authors want to acknowledge the entire HERMES project consortium, composed of the Italian Space Agency (ASI), Italian Institute of Astrophysics (INAF), Politecnico di Milano, Cagliari University, National Institute of Higher Mathematics (INdAM), Skylabs Technology, Deimos Space, Nova Gorica University, Tubingen University, Loránd Eötvös University, Aalta Lab, and C3S Electronics. The authors want to acknowledge the European Commission for the funding of the HERMES project in the Horizon 2020 framework under Grant agreement ID: 821896. The authors declare that they have no conflicts of interest.

References

1. F. Fiore et al., "HERMES: a swarm of nano-satellites for high energy astrophysics and fundamental physics," *Proc. SPIE* **10699**, 106992Q (2018).
2. F. Fuschino et al., "HERMES: an ultra-wide band x and gamma-ray transient monitor on board a nano-satellite constellation," *Nucl. Instrum. Methods Phys. Res. Sect. A* **936**, 199–203 (2019).
3. C. Pardini and L. Anselmo, "Decay of spherical satellites," *J. Astronaut. Sci.* **49**(2), 255–268 (2001).
4. C. Pardini, W. K. Tobiska, and L. Anselmo, "Analysis of the orbital decay of spherical satellites using different solar flux proxies and atmospheric density models," *Adv. Space Res.* **37**(2), 392–400 (2006).
5. F. Lemoine et al., "The development of the joint NASA GSFC and the National Imagery and Mapping Agency (NIMA) Geopotential Model EGM96," Tech. Rep. NASA TP—1998–206861, NASA—Goddard Space Flight Center (1998).
6. European Cooperation for Space Standardization (ECSS), "Space engineering – space environment," Standard E-ST-10-04C, ECSS (2008).
7. W. M. Folkner et al., "The planetary and lunar ephemerides DE430 and DE431," *Interplanet. Network Prog. Rep.* **196**(42), 1–81 (2014).
8. L. G. Jacchia, "New static models of the thermosphere and exosphere with empirical temperature profiles," Special Report 313, Smithsonian Institution Astrophysical Observatory (SAO) (1970).
9. C. E. Roberts, "An analytic model for upper atmosphere densities based upon Jacchia's 1970 models," *Celestial Mech.* **4**(3-4), 368–377 (1971).
10. NOAA, "Space weather prediction center," 2017, http://https://www.swpc.noaa.gov/ (accessed 2017-09-30).
11. K. Alfriend et al., *Spacecraft Formation Flying: Dynamics, Control and Navigation*, Elsevier Astrodynamics Series (2009).
12. D. P. Scharf, F. Y. Hadaegh, and S. R. Ploen, "A survey of spacecraft formation flying guidance and control (part 1): guidance," in *Proc. 2003 Am. Control Conf., 2003*, Vol. 2, pp. 1733–1739 (2003).
13. C. Meegan et al., "The Fermi gamma-ray burst monitor," *Astrophys. J.* **702**, 791–804 (2009).
14. D. Gruber et al., "The Fermi GBM gamma-ray burst spectral catalog: four years of data," *Astrophys. J. Suppl. Ser.* **211**(1), 12 (2014).
15. A. Colagrossi et al., "Semi-analytical approach to fasten complex and flexible pointing strategies definition for nanosatellite clusters: the HERMES mission case from design to flight," in *70th Int. Astronaut. Congr., 21–25 October 2019*, Washington D.C. (2019).
16. J. Kennedy and R. Eberhart, "Particle swarm optimization," in *Proc. ICNN'95, Int. Conf. Neural Networks*, Perth, Western Australia (1995).
17. R. H. Byrd, M. E. Hribar, and J. Nocedal, "An interior point algorithm for large-scale nonlinear programming," *SIAM J. Optim.* **9**(4), 877–900 (1999).
18. J. M. Hanson and B. B. Beard, "Applying Monte Carlo simulation to launch vehicle design and requirements analysis," Tech. Rep. NASA TP—2010–216447, NASA—Marshall Space Flight Center (2010).

Andrea Colagrossi is a postdoctoral research fellow at the Aerospace Science and Technology Department of Politecnico di Milano. He is responsible for the GNC subsystem and the mission analysis of the HERMES project. He is an author and a co-author of about 20 scientific publications on GNC, small space systems, and non-Keplerian dynamics. He has been involved in national and EU/ESA-funded projects for developing innovative techniques for spacecraft GNC.

Jacopo Prinetto is a PhD candidate at the Aerospace Science and Technology Department of Politecnico di Milano. He is an author and a co-author of about 10 scientific publications on low-thrust trajectory design and optimization. He has been involved in national and EU/ESA-funded projects in the role of mission analyst.

Stefano Silvestrini is a PhD candidate at the Aerospace Science and Technology Department of Politecnico di Milano. He is an author and a co-author of about 15 scientific publications on AI-based GNC, distributed systems, and relative dynamics. He has been involved in national and EU/ESA-funded projects for developing innovative techniques for spacecraft GNC in different scenarios, such as missions to small bodies and proximity operations for debris removal.

Michèle Lavagna is a full professor in flight mechanics at the Aerospace Science and Technology Department of Politecnico di Milano. She is the head of the ASTRA Team Research Group. She is an author and a co-author of more than 300 scientific publications on space engineering topics. She has been the supervisor of 27 PhD research studies and 149 master's theses in space engineering.